

Structural and corrosion characterization of biodegradable Mg-Zn alloy castings

J. Kubásek*, D. Vojtěch, I. Pospíšilová

*Department of Metals and Corrosion Engineering, Institute of Chemical Technology, Prague,
Technická 5, 166 28 Prague 6, Czech Republic*

Received 20 February 2012, received in revised form 3 May 2012, accepted 4 May 2012

Abstract

As-cast Mg, Mg-1Zn, Mg-4Zn and Mg-6Zn (wt.%) alloys were studied in this work. The alloys were prepared by gravity casting into a metal mold. The average cooling rate was 500 K min^{-1} . Structural analysis revealed the presence of zinc concentration gradients and a strong zinc super-saturation in the α -Mg phase. In the Mg-4Zn and Mg-6Zn alloys, an interdendritic MgZn phase was present. The alloys' Vickers hardness increased with increasing Zn-concentration from 25 HV10 (pure Mg) to 45 HV10 (Mg-6Zn). The corrosion rates were measured by exposure to simulated body fluid. The Mg-1Zn alloy showed the lowest corrosion rate of $0.08 \text{ mm year}^{-1}$, which was significantly lower than the corrosion rates of pure Mg and AZ91HP alloys (0.5 and 0.6 mm year^{-1} , respectively). Increasing the Zn concentration in Mg alloys increased the corrosion rate, and the as-cast Mg-6Zn alloy corroded quickly, at a rate of 3 mm year^{-1} . The alloys were solution heat treated at 300°C for 150 h. Structural analysis revealed a partial dissolution of the MgZn phase, precipitation of the MgZn phase in regions that were originally supersaturated with zinc, and homogenization of the α -Mg phase during the heat treatment process. The observed structural changes increased the corrosion resistance, particularly that of the Mg-6Zn alloy whose corrosion rate was reduced four-fold, to 0.8 mm year^{-1} . The measured corrosion rates were related to the observed structural characteristics of the alloy materials.

Key words: magnesium alloys, biomaterials, corrosion, casting

1. Introduction

Magnesium alloys exhibit good specific strength and biocompatibility, making them of interest for biodegradable medical implants, like fixation devices for fractured bones or stents. Magnesium is advantageous because it has similar mechanical properties and density as natural bone. In contrast to standard bone fixation devices that are made of bio-inert stainless steels or Ti alloys, biodegradable devices function as temporary fixators because they progressively degrade in biological environments into non-toxic compounds that are readily excreted by the body. After the bone healing process is complete, no second surgery is needed to remove a biodegradable fixation device, which reduces the inconvenience and the health care costs for patients. Over the past few decades, researchers

have been interested in finding Mg-based materials whose degradation rates are sufficiently low to allow complete healing of the defect, while also minimizing the negative side effects of the degradation products, namely hydrogen and alkalinity. Suitable biodegradable magnesium alloys are difficult to find because they require complex knowledge of magnesium metallurgy, chemistry and biology. For this reason, no commercial magnesium biodegradable implants have been approved. In human medicine, biodegradable devices are dominated by polymeric materials, such as polylactic acid (PLA). However, the use of magnesium alloys for load-bearing implants, like fixation screws or plates, is still a challenge because these alloys show significantly higher strength than polymers.

Pure magnesium is not suitable for biodegradable bone fixation devices because it has low mechanical

*Corresponding author: tel.: +420 736278401; fax: +420 220444400; e-mail address: Kubasek.jiri@gmail.com

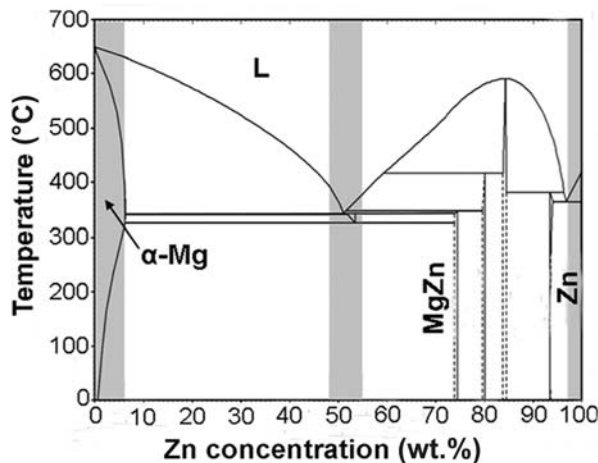


Fig. 1. The Mg-Zn binary phase diagram [19] with marked regions representing Mg-Zn-based biodegradable alloys that have been studied so far.

strength. Therefore, magnesium alloys have been considered for these applications. Until recently, studies of biodegradable magnesium based alloys have been focused on AZ (Mg-Al-Zn), AM (Mg-Al-Mn), AE (Mg-Al-RE), ZE (Mg-Zn-RE), WE (Mg-Y-RE), MZ (Mg-Mn-Zn), WZ (Mg-Y-Zn), LAE (Mg-Li-Al-RE), ZK (Mg-Zn-Zr), Mg-Ca and Mg-Zn-Ca alloys (according to ASTM designation, RE-rare earths) [1–3]. The majority of these alloys were originally developed for engineering applications in the automotive and aerospace industries. However, for biomaterial applications, alloy elements must be selected more carefully to minimize or avoid potential toxic elements. For this reason, the majority of recent research has focused on magnesium alloys containing elements generally considered “less problematic” for biocompatibility, mainly zinc, calcium, rare earths, yttrium, zirconium, manganese and silicon [4–13]. Among these alloy elements, zinc is essential.

Zinc, as a more noble metal than magnesium, is known to increase the corrosion resistance and strength of Mg. Zinc is important for biological functions: it supports the immune system, normal growth and a proper sense of taste and smell [7, 14]. The recommended dietary allowance (RDA) and the recommended upper limit for zinc intake are 15 and 40 mg per day, respectively [15]. Consuming zinc in amounts higher than these values, up to 100 mg day⁻¹, is considered relatively non-toxic and can be tolerated for some time [15].

The binary Mg-Zn phase diagram is shown in Fig. 1. Three regions are marked in this diagram, representing Mg-Zn-based biodegradable alloys that have been studied so far. The first region includes alloys containing up to approximately 6 wt.% Zn, which is the solubility limit of Zn in Mg. Structures of these al-

loys are dominated by an $\alpha(\text{Mg})$ solid solution, which ensures a good formability at elevated temperatures. For this reason, the low-Zn alloy materials are usually formed into their final shapes by hot-extrusion. Multiple papers have reported that these materials show good strength, corrosion resistance and biocompatibility. The second group of alloys has a chemical composition that approaches the deep eutectic point in the Mg-Zn system. This group of alloys shows a high glass forming ability, as they readily form an amorphous phase when the melt is rapidly cooled. Even though amorphous Mg-Zn-based alloys were recently reported to have excellent strength, corrosion resistance and biocompatibility properties [16, 17], they are not easily prepared in bulk. The third group of materials represents zinc-based alloys, in which magnesium concentrations do not exceed 3 wt.%, which corresponds to the eutectic point. These alloys were studied only recently by our team [18]. We have shown that the corrosion resistance of these Zn-Mg alloys is significantly better than that of magnesium alloys, and that their strength in the as-cast state is much higher than that of PLA.

In this study we focused our attention on the low-zinc Mg-Zn alloys (up to 6 wt.% Zn). These alloys were commonly studied in the as-extruded state. It is generally acknowledged that zinc positively influences the corrosion resistance and mechanical strength of these alloys. Precise gravity casting, or die casting are alternative processes for preparing small implants made of Mg-Zn alloys, like screws, nails or plates. The casting process enables the production of complex-shaped components in one step. However, little information is available about how zinc affects the properties of these as-cast biodegradable Mg-Zn alloys. Therefore, our study provides information about the structural and corrosion parameters of Mg-Zn alloys when they are gravity cast into a small metal mold. We show that zinc affects the corrosion in a complicated way, based on its concentration and spatial distribution within the structure.

2. Materials and methods

Four alloys with nominal compositions of Mg, Mg-1Zn, Mg-4Zn and Mg-6Zn were studied (all concentrations are given in wt.%). Chemical compositions are summarized in Table 1. The alloys were prepared by melting pure magnesium (purity of 99.7 %, composition given in Table 1) and high purity zinc (99.99 %) in a vacuum induction furnace under argon at ambient pressure to prevent the oxidation of magnesium and the excessive evaporation of zinc. After 10 min of homogenization at 730°C, the melt was poured into a cast iron metal mold to prepare a cylindrical casting 50 mm in length and 20 mm in diameter. The average cooling rate was 500 K min⁻¹, as measured by a

Table 1. Chemical composition of the investigated alloys (in wt.%)

Alloy	Concentration (wt.%)									
	Al	Si	K	Ca	Mn	Fe	Ni	Cu	Zn	Mg
Mg	0.0880	0.0407	0.0114	0.0067	0.0131	0.0045	0.0036	0.0226	0.0485	bal.
Mg-1Zn	0.0230	0.0410	0.0250	0.0130	0.0130	0.0070	–	0.0295	1.4440	bal.
Mg-4Zn	0.0273	0.0565	–	–	0.0101	0.0072	–	0.0308	3.7940	bal.
Mg-6Zn	0.0478	0.0489	–	0.0077	0.0077	0.0062	0.0046	0.0250	5.6985	bal.
Mg-9Al-1Zn	8.8551	0.0701	0.0032	0.0057	0.0123	<0.0030	<0.0030	<0.0030	0.8962	bal.

Table 2. Chemical composition of the SBF used in this study [20]

Compound	NaCl	KCl	CaCl ₂	NaHCO ₃	glucose	MgSO ₄ ·7H ₂ O	KH ₂ PO ₄	Na ₂ HPO ₄ ·12H ₂ O
Concentration (g l ⁻¹)	8	0.4	0.14	0.35	1	0.2	0.09	0.08

thermocouple placed in the middle of the mold. The chemical compositions and homogeneity of the castings were verified on both ends of the sample. Differences in Zn concentrations between the sample ends did not exceed 0.05 %.

To determine the effect of zinc distribution on the corrosion and mechanical characteristics of the alloys, some of the castings were solution heat treated, i.e., annealed at 300 °C for 150 h, followed by water quenching. The heat treatment temperature was optimized according to the Mg-Zn phase diagram in Fig. 1, where the eutectic temperature is 340 °C. A long annealing time (150 h) was necessary because of the relatively low temperature (300 °C).

The corrosion behavior of the alloys was studied by immersion tests in a simulated body fluid (SBF) whose composition is given in Table 2. Coupons (20 mm in diameter, 2 mm thick) were immersed in 200 ml of SBF for 336 h at 37 °C. To prevent the evaporation of SBF corrosion tests were carried out in closed vessels. After corrosion tests, corrosion products were removed using a solution of 200 g l⁻¹ CrO₃, 10 g l⁻¹ AgNO₃ and 20 g l⁻¹ Ba(NO₃)₂, according to ISO 8407. The corrosion rates were calculated (mm yr⁻¹) using the weight losses measured on a balance with an accuracy of 0.1 mg, according to ASTM G31-72. Each immersion test was performed four times to ensure sufficient statistics. The corrosion rates of the Mg-Zn alloys were compared to that of a high purity extruded Mg-9Al-1Zn (AZ91HP) alloy whose chemical composition is also given in Table 2. It is known that hot extrusion refines and homogenizes the structure of Mg alloys, resulting in better corrosion resistance. Therefore, the AZ91HP alloy served as a corrosion resistant standard in this study.

The structure and elemental distributions of the as-cast and heat-treated alloys, as well as the corroded surfaces, were studied by light microscopy (LM)

and scanning electron microscopy (SEM, Tescan Vega 3) with energy dispersion spectrometry (EDS, Oxford Instruments Inca 350). Prior to the LM study, the samples were etched with a solution containing 70 ml of picric acid, 10 ml of acetic acid and 10 ml of water. The phase composition was determined by X-ray diffraction (XRD, X Pert Pro). Mechanical properties were characterized by Vickers hardness measurements with a loading of 5 kg.

3. Results and discussion

3.1. Structure and hardness

Light micrographs of the as-cast Mg-Zn alloys are shown in Fig. 2. The pure Mg sample contained grains elongated in the direction of heat removal (Fig. 2a). The as-cast Mg-Zn alloys show primary α -Mg dendrites (light) surrounded by inter-dendritic regions rich in zinc (dark) (Figs. 2b–d). The average dendrite arm spacing is approximately 20 μ m, suggesting a relatively high cooling rate during casting. The inter-dendritic regions in the Mg-3Zn and Mg-6Zn contain an MgZn phase (black particles) whose volume fraction increases with increasing zinc content in the alloy. In the Mg-6Zn alloy, elongated MgZn particles form an almost continuous network along the dendrite boundaries. In contrast, the only structural constituent of the Mg-1Zn alloy is the α -Mg phase that contains all of the dissolved zinc. The structure of the AZ91HP alloy (Fig. 2e) was recrystallized and contained equiaxial grains of α -Mg (light) and fine micrometer-sized particles of the Al₁₂Mg₁₇ intermetallic phase (dark), located mainly along the α -Mg grain boundaries.

Figure 3 shows the influence of solution heat treatment at 300 °C/150 h on the alloys. The dendritic morphology and inter-dendritic network in the Mg-Zn al-

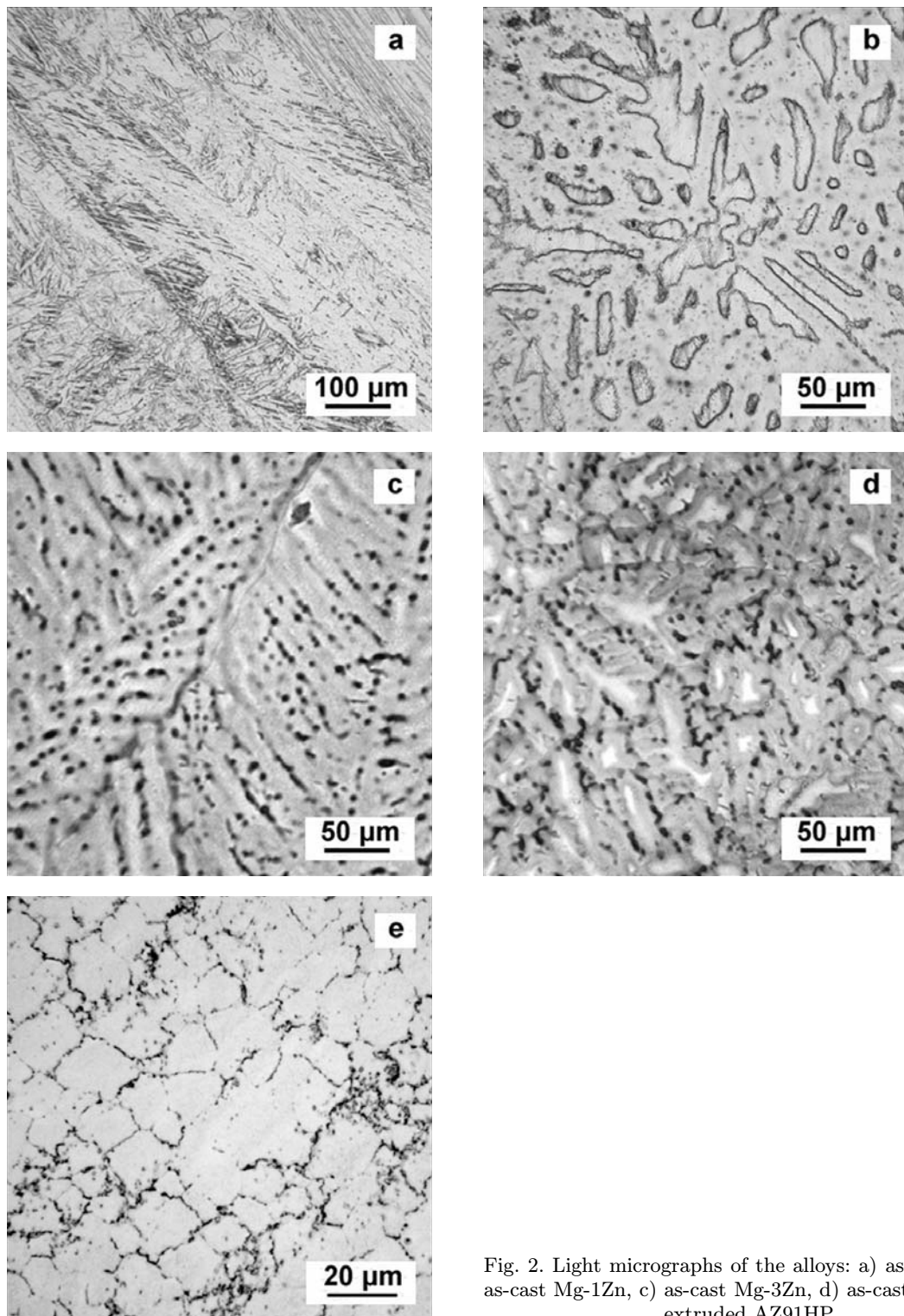


Fig. 2. Light micrographs of the alloys: a) as-cast Mg, b) as-cast Mg-1Zn, c) as-cast Mg-3Zn, d) as-cast Mg-6Zn, e) extruded AZ91HP.

loys vanished during the heat treatment. Surprisingly, despite the long annealing time (150 h), the resulting structures were not fully homogeneous, suggesting that a small part of the inter-dendritic MgZn phase remained undissolved in the α -Mg phase. This phase appeared as dark particles. Apparently, the annealing temperature of 300 °C was too low to sufficiently accel-

erate solid state diffusion and to drive complete dissolution (Fig. 1). In addition to the inter-dendritic MgZn phase formed during solidification, large areas containing fine dark particles appeared in the structure after heat treatment (Fig. 3). In these areas, precipitation occurred and produced fine MgZn particles. It seems surprising that precipitation could occur above

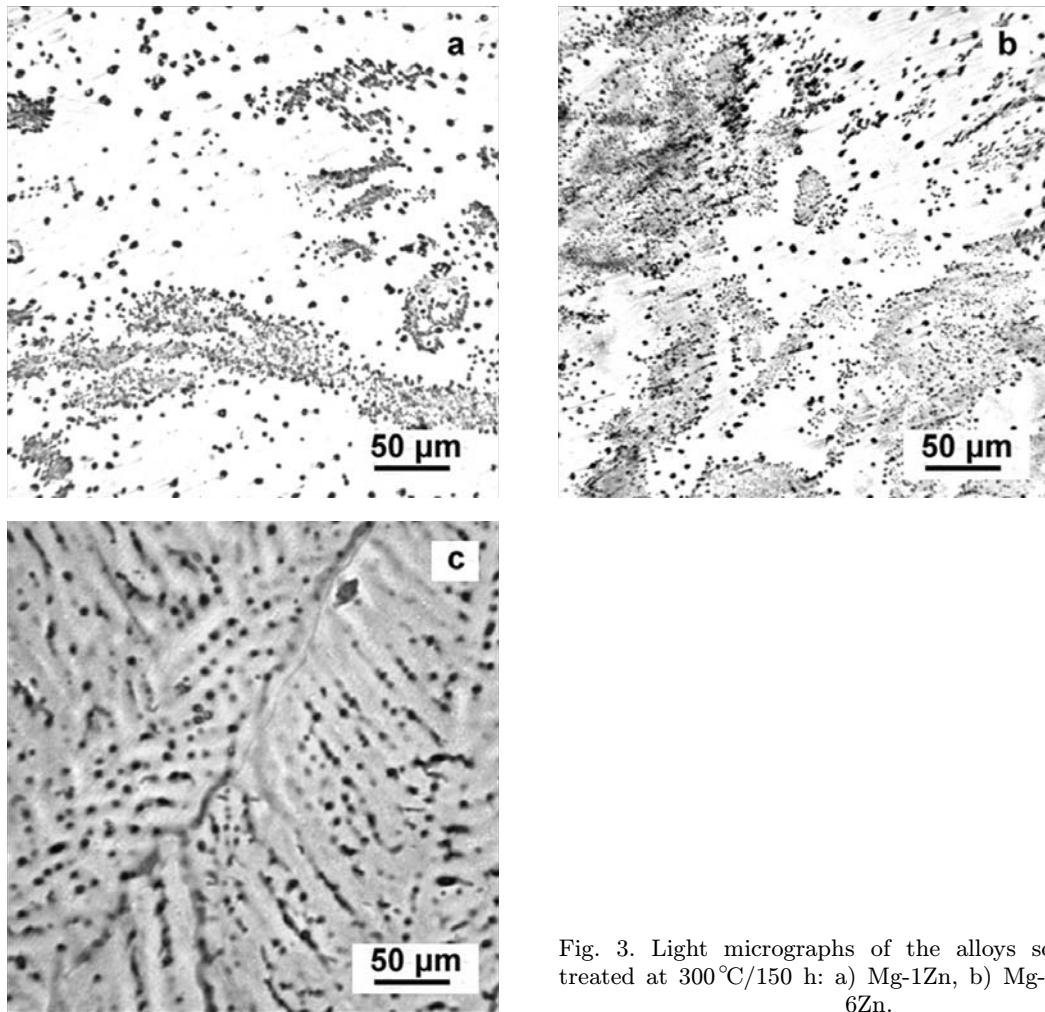


Fig. 3. Light micrographs of the alloys solution heat treated at 300°C/150 h: a) Mg-1Zn, b) Mg-3Zn, c) Mg-6Zn.

the solvus temperature (Fig. 1), but, as will be shown later, this precipitation is caused by a strong supersaturation of the α -Mg phase with zinc.

Elemental mapping and a detailed chemical microanalysis were performed by EDS to determine zinc distributions in the as-cast and heat-treated alloys. This is illustrated by elemental maps of the Mg-6Zn alloy, shown in Fig. 4. In Fig. 4a, the as-cast alloy exhibits both Zn-depleted α -Mg dendrites (dark) and Zn-enriched inter-dendritic regions (light). In the α -Mg dendrites, the zinc is not uniformly distributed, as shown by a concentration gradient between the dendrite core and its edges. Table 3 summarizes the zinc concentrations found at various points in Fig. 4. The Zn concentration in the dendrite cores was relatively low and did not significantly exceed 3 % (points 1–4), whereas the Zn concentration near the inter-dendritic phase was greater than 10 % (points 5–8). It should be noted that this concentration significantly exceeded the maximum Zn solubility in Mg (6 %), implying that the α -Mg phase near the dendrite edges is unstable and is prone to decomposition when heated at 300°C to form a solid solution with approximately 6 % Zn

(Fig. 1). This process occurs by precipitation of the MgZn phase, as shown in Fig. 3. It is likely that extending the annealing time at 300°C would allow the MgZn phase to fully dissolve in Mg, but long annealing times are not practical. Figure 4a and Table 3 also show that the light inter-dendritic regions contain between 30 and 60 % Zn (points 9–13). Taking into account that the chemical microanalysis of fine particles may be influenced by the surrounding α -Mg phase, these values approach the Zn concentrations found in the α -Mg + MgZn eutectics (51 % Zn) and in the MgZn phase (74 % Zn) (Fig. 1), suggesting that the MgZn phase predominates in these regions. The presence of Zn concentration gradients in the α -Mg phase, super-saturation of α -Mg with zinc and the presence of the MgZn inter-dendritic phase all result from a fast cooling rate (500 K min⁻¹) during solidification, which thus occurs far from equilibrium.

As stated before, the solution heat treatment temperature and time were too low to cause total dissolution of the MgZn phase. In Fig. 4b, the remaining MgZn phase is shown by the light particles distributed within the dark α -Mg matrix. As in the previous

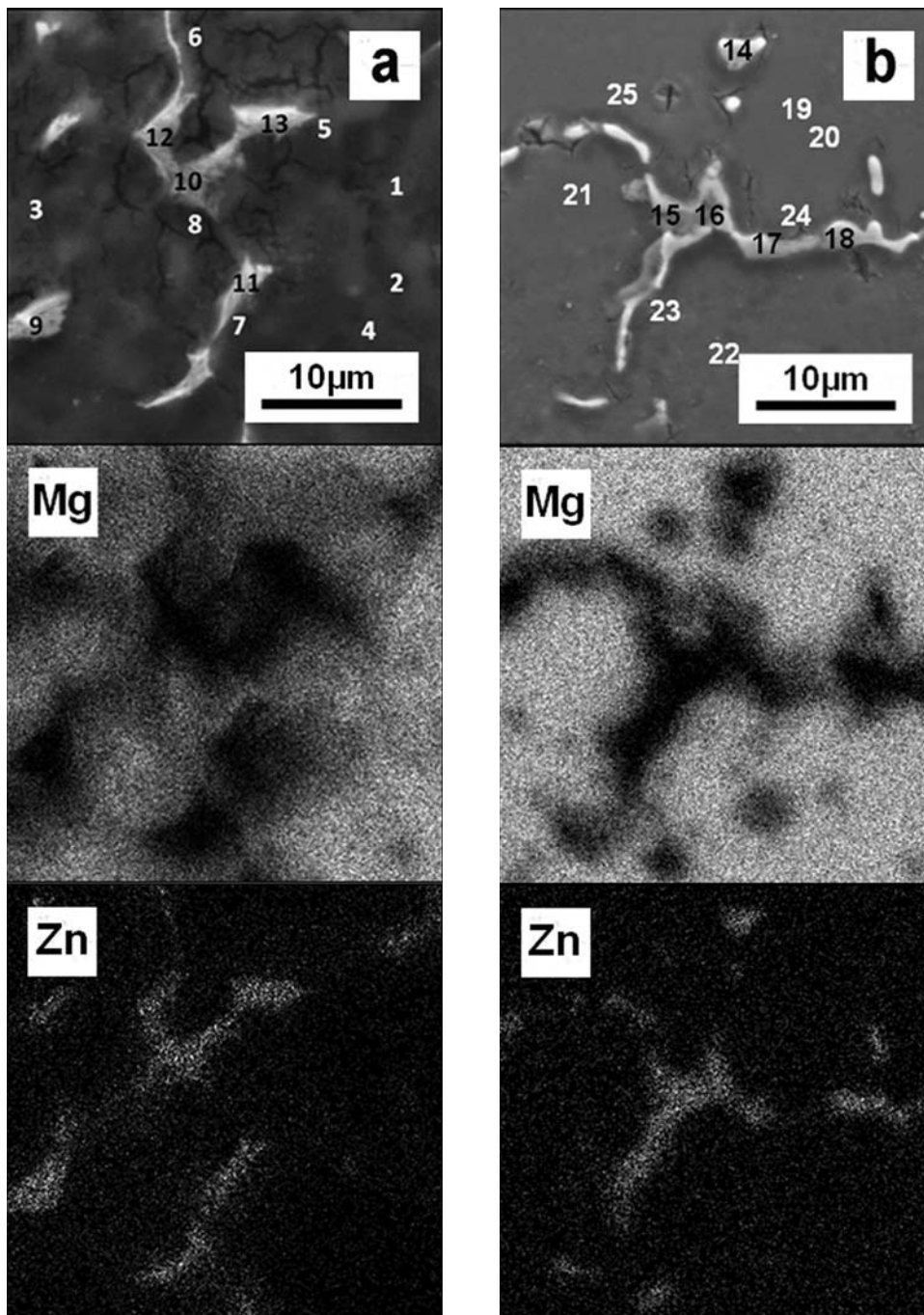


Fig. 4. Elemental maps of the Mg-6Zn alloy: a) as-cast, b) solution heat-treated at 300°C/150 h. Chemical compositions in marked points are summarized in Table 3.

case, Zn concentrations measured in these particles ranged from 30 to 60 % (points 14–18), as shown in Table 3. The main difference between the as-cast and heat-treated alloy is the zinc distribution in the α -Mg phase. The as-cast state is characterized by Zn concentration gradients (Fig. 4a), but these gradients vanished during heat treatment. Table 3 shows that Zn is distributed in the α -Mg phase almost uniformly after heat treatment, at a concentration of about 5 % (points 19–26 in Fig. 4b), which is close to the zinc

solid solubility at 300°C (Fig. 1). Homogeneous zinc distribution in the α -Mg phase is also observed in the solution heat-treated Mg-1Zn and Mg-4Zn alloys. The observed structural change also has a direct impact on the corrosion behavior of the Mg-Zn alloys.

Figure 5 illustrates the development of Vickers hardness as a function of the zinc content in the alloy, which is directly related to the observed structures. As expected, the hardness of both the as-cast and annealed alloys increased slightly with an increasing

Table 3. Results of chemical microanalysis of the as-cast and solution heat-treated Mg-6Zn alloy (chemical compositions for the points marked in Figs. 4a,b) (EDS)

As-cast		Solution heat treated at 300°C/150 h	
point no.	Zn concentration	point no.	Zn concentration
1	2.55	14	33.56
2	3.62	15	44.00
3	3.01	16	48.18
4	2.87	17	60.16
5	8.19	18	39.61
6	10.65	19	4.97
7	9.32	20	5.11
8	9.76	21	5.01
9	37.70	22	5.45
10	42.82	23	5.26
11	60.28	24	6.24
12	35.20	25	6.04
13	51.33	26	5.38

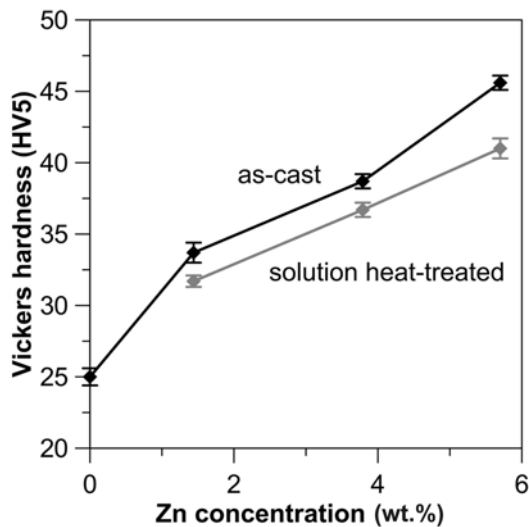


Fig. 5. Vickers hardness of the alloys versus the Zn-concentration.

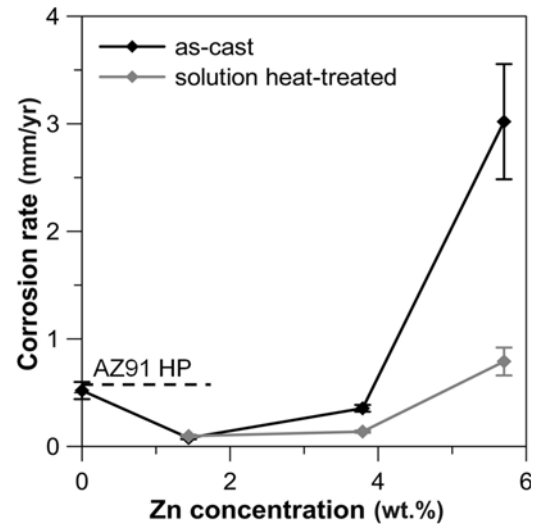


Fig. 6. Corrosion rates of the as-cast and solution heat-treated alloys versus zinc concentration.

Zn concentration. The pure Mg had a hardness of 25 HV5, whereas the as-cast Mg-6Zn alloy had a value of 45 HV5. Zinc contributes to alloy hardening in two ways: 1. zinc dissolved in α -Mg causes solid solution hardening, and 2. MgZn particles also cause hardening of the alloy. Figure 5 demonstrates that the effect of solution annealing on hardness is negligible. The differences between the as-cast and heat-treated alloys are only a few units of HV5. Although the partial dissolution of the hard, inter-dendritic MgZn phase may lead to some softening of the alloy, this effect is probably counteracted by the precipitation of MgZn particles in areas that are supersaturated with zinc (Fig. 3). The AZ91HP alloy has the highest hardness value (61 HV5) out of all the investigated materials,

mainly due to a high concentration of aluminum that causes both solid solution hardening and hardening by the $\text{Al}_{12}\text{Mg}_{17}$ phase.

3.2. Corrosion resistance

Figure 6 shows the corrosion rates for the as-cast and solution heat-treated alloys in SBF (Table 2). It is clear that the corrosion rate of the alloys strongly depends on the zinc concentration. Although pure magnesium has a corrosion rate of approximately 0.5 mm year⁻¹ (similar to the AZ91HP alloy), the addition of only 1.4% of zinc reduces the corrosion rate by almost an order of magnitude, to approximately 0.08 mm year⁻¹. Zinc's ability to improve the alloy's corrosion

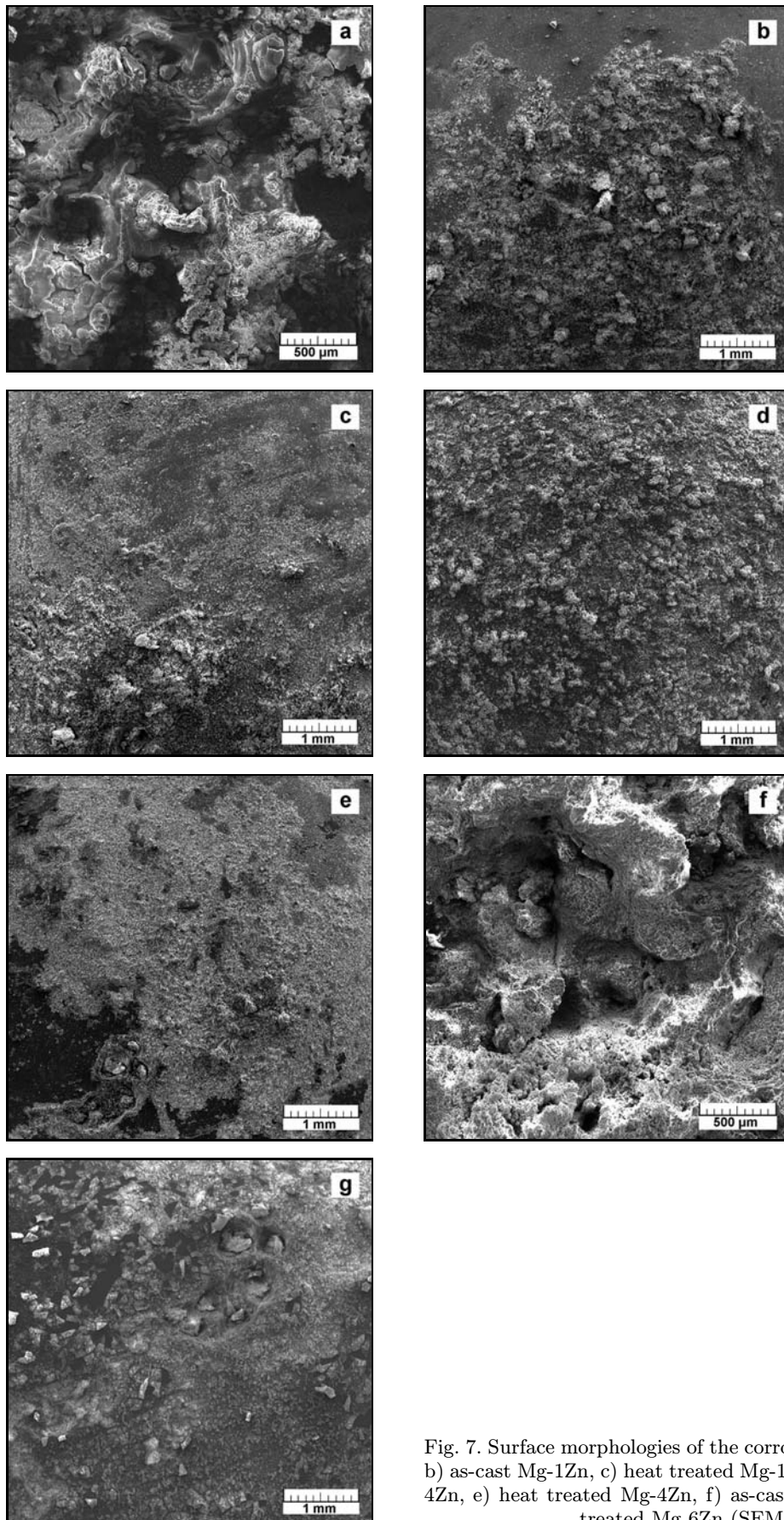
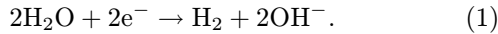


Fig. 7. Surface morphologies of the corroded alloys: a) Mg, b) as-cast Mg-1Zn, c) heat treated Mg-1Zn, d) as-cast Mg-4Zn, e) heat treated Mg-4Zn, f) as-cast Mg-6Zn, g) heat treated Mg-6Zn (SEM).

resistance is caused by two factors: 1. Zinc is significantly more noble than magnesium. The standard potentials of Zn and Mg are -0.762 and -2.372 V (versus the Standard Hydrogen Electrode), respectively [21]; and 2. Zinc is characterized by a relatively high hydrogen over-potential [21]. It is well known that hydrogen gas is the main product of magnesium corrosion in SBF. It is formed by the following cathodic reaction [7, 22]:



Therefore, it can be assumed that the kinetics of hydrogen gas evolution is reduced by the presence of zinc in the α -Mg solid solution. Figure 2 shows that the as-cast Mg-1Zn alloy does not contain an MgZn secondary phase in its structure. Despite concentration gradients observed in α -Mg dendrites, the effect of galvanic cells between more and less noble structural components is minimal in this alloy. The relatively high corrosion rate of the AZ91HP alloy is caused by a high volume fraction of intermetallic phases, which are more noble than magnesium (Fig. 2e) [22]. When the as-cast Mg-Zn alloy contained 4 % Zn, the corrosion rate was approximately four fold higher (0.36 mm year $^{-1}$). As illustrated in Fig. 2, the structure of this alloy exhibited an inter-dendritic MgZn phase. This phase contained more than 70 % Zn and was therefore significantly more noble than the α -Mg matrix. The galvanic micro-cells between the structural constituents accelerated the corrosion. The negative effect of the MgZn phase on the alloy's corrosion resistance was clearly observed in the Mg-6Zn alloy, whose corrosion rate was 3 mm year $^{-1}$, almost one order of magnitude higher than the Mg-4Zn alloy.

Figure 6 demonstrates that the corrosion resistance of the Mg-Zn alloys, particularly those with a higher Zn-concentration, can be positively modified by heat treatment. Heat treating the Mg-6Zn alloy reduced the corrosion rate nearly four-fold, from 3 mm year $^{-1}$ to 0.8 mm year $^{-1}$. Similarly, the heat-treated Mg-4Zn alloy showed an almost three times lower corrosion rate compared to the as-cast state. The positive influence of heat treating the alloys is evident from observing the alloy surfaces after corrosion testing (Fig. 7). The pure magnesium sample (Fig. 7a) was covered in thick, porous corrosion products, dominated by $\text{Mg}(\text{OH})_2$, as shown by XRD and EDS (not shown). The surface morphology of the corrosion products ($\text{Mg}(\text{OH})_2$) for the as-cast and heat-treated Mg-1Zn alloys was similar (Figs. 7b,c). In contrast, the as-cast Mg-4Zn and Mg-6Zn (Figs. 7d and 7f) were covered by massive layers of corrosion products that were thicker than those on their solution heat-treated counterparts (Figs. 7e and 7g).

The positive influence of the solution heat treatment can be directly related to the observed structural

modifications. Figure 2 shows that this treatment led to a partial dissolution of the coarse MgZn phase from the solidification process. In addition, very fine MgZn particles precipitated in relatively large areas. Therefore, the heat treatment caused the coarse heterogeneous as-cast structure with a nearly continuous MgZn network to be replaced by a more homogeneous distribution of zinc and noble MgZn phase within the structure. The effect of galvanic corrosion was thus diminished for this heat-treated structure. A recent report [8] compared as-cast and hot-extruded ZK60 (Mg-6Zn-Zr) alloys. The latter showed a better corrosion performance because it exhibited a more uniform structure. The absence of an MgZn phase in the as-cast Mg-1Zn alloy caused the heat treatment to have a negligible effect on the corrosion of this alloy (Fig. 6).

4. Conclusions

This work presents evidence that small Mg-Zn castings that are solidified in metal molds (with relatively high cooling rates) are characterized by strongly non-equilibrium structures, including the presence of concentration gradients and zinc supersaturation in the magnesium phase. These characteristics increase the structural heterogeneities within the alloys. For this reason, only relatively low levels of zinc improve the alloy's corrosion resistance. At Zn concentrations above 1 %, the corrosion rate increased progressively with the amount of Zn, due to the presence of a MgZn phase that created micro-galvanic cells with the surrounding α -Mg matrix. The high observed corrosion rate of the as-cast Mg-6Zn alloy is attributed to this type of galvanic corrosion. Although large concentrations of zinc diminish the corrosion resistance of as-cast alloys, the effects of Zn on hardness and strength are beneficial. For this reason, heat treatment of these alloys at 300°C should be applied to homogenize the structure and to improve the corrosion resistance of the as-cast high-zinc-content Mg-Zn alloys. A similar effect should be expected in the case of hot extruded Mg-Zn alloys, provided that hot extrusion is performed under properly controlled conditions.

Acknowledgement

The research of biodegradable Mg-based alloys was financially supported by the Czech Science Foundation under the project no. P108/12/G043 and by the Academy of Sciences of the Czech Republic (project no. KAN300100801).

References

- [1] Zeng, B. R., Dietzel, W., Witte, F., Hort, N., Blawert, C.: *Adv. Eng. Mater.*, 10, 2008, p. B3.
[doi:10.1002/adem.200800035](https://doi.org/10.1002/adem.200800035)

- [2] Witte, F.: *Acta Biomater.*, 6, 2010, p. 1680. PMID: 20172057. [doi:10.1016/j.actbio.2010.02.028](https://doi.org/10.1016/j.actbio.2010.02.028)
- [3] Vojtěch, D., Čížová, H., Volenec, K.: *Kovove Mater.*, 44, 2006, p. 211.
- [4] Gu, X. N., Zheng, Y. F.: *Front. Mater. Sci. China*, 4, 2010, p. 111. [doi:10.1007/s11706-010-0024-1](https://doi.org/10.1007/s11706-010-0024-1)
- [5] Staiger, M. P., Pietak, A. M., Huadmai, J., Dias, G.: *Biomaterials*, 27, 2006, p. 1728. PMID:16246414. [doi:10.1016/j.biomaterials.2005.10.003](https://doi.org/10.1016/j.biomaterials.2005.10.003)
- [6] Xin, Y., Hu, T., Chu, P. K.: *Acta Biomater.*, 7, 2011, p. 1452. PMID:21145436. [doi:10.1016/j.actbio.2010.12.004](https://doi.org/10.1016/j.actbio.2010.12.004)
- [7] Witte, F., Hort, N., Vogt, C., Cohen, S., Kainer, K. U., Willumeit, R., Feyerabend, F.: *Curr. Opin. Solid State Mater. Sci.*, 12, 2008, p. 63. [doi:10.1016/j.cossms.2009.04.001](https://doi.org/10.1016/j.cossms.2009.04.001)
- [8] Gu, N. X., Li, N., Zheng, Y. F., Ruan, L.: *Mater. Sci. Eng. B*, 176, 2011, p. 1778. [doi: 10.1016/j.mseb.2011.05.032](https://doi.org/10.1016/j.mseb.2011.05.032).
- [9] Zhang, S., Zhang, X., Zhao, C., Li, J., Song, Y., Xie, C., Tao, H., Zhang, Y., He, Y., Jiang, Y.: *Acta Biomater.*, 6, 2010, p. 626. PMID:19545650. [doi:10.1016/j.actbio.2009.06.028](https://doi.org/10.1016/j.actbio.2009.06.028)
- [10] Huan, Z. G., Leeflang, M. A., Zhou, J., Fratila-Apachitei, R. E., Duszczuk, J.: *J. Mater. Sci. Mater. Med.*, 21, 2010, p. 2623. PMID:20532960, PMCID:2935537. [doi:10.1007/s10856-010-4111-8](https://doi.org/10.1007/s10856-010-4111-8)
- [11] Hänzi, A. C., Gerber, I., Schinhammer, M., Löffler, J. F., Uggowitzer, P. J.: *Acta Biomater.*, 6, 2010, p. 1824. PMID:19815099. [doi:10.1016/j.actbio.2009.10.008](https://doi.org/10.1016/j.actbio.2009.10.008)
- [12] Zhang, E., Yang, L.: *Mater. Sci. Eng. A*, 497, 2008, p. 111. [doi:10.1016/j.msea.2008.06.019](https://doi.org/10.1016/j.msea.2008.06.019)
- [13] Stulikova, I., Smola, B.: *Mater. Charact.*, 61, 2010, p. 952. [doi:10.1016/j.matchar.2010.06.004](https://doi.org/10.1016/j.matchar.2010.06.004)
- [14] Li, Z., Gu, X., Lou, S., Zheng, Y.: *Biomaterials*, 29, 2008, p. 1329. PMID:18191191. [doi:10.1016/j.biomaterials.2007.12.021](https://doi.org/10.1016/j.biomaterials.2007.12.021)
- [15] Fosmire, G. J.: *Am. J. Clin. Nutr.*, 51, 1990, p. 225. PMID:2407097.
- [16] Zberg, B., Uggowitzer, P. J., Löffler, J. F.: *Nat. Mater.*, 8, 2009, p. 887. PMID:19783982. [doi:10.1038/nmat2542](https://doi.org/10.1038/nmat2542)
- [17] Gu, X., Zheng, Y., Zhong, S., Xi, T., Wang, J., Wang, W.: *Biomaterials*, 31, 2010, p. 1093. PMID:19939446. [doi:10.1016/j.biomaterials.2009.11.015](https://doi.org/10.1016/j.biomaterials.2009.11.015)
- [18] Vojtěch, D., Kubásek, J., Šerák, J., Novák, P.: *Acta Biomater.*, 7, 2011, p. 3515. PMID:21621017. [doi:10.1016/j.actbio.2011.05.008](https://doi.org/10.1016/j.actbio.2011.05.008)
- [19] Gale, W. F., Totemeiner, T. C.: *Smithells Metals Reference Book*. 8th ed. Oxford, Elsevier 2004.
- [20] Wang, H., Shi, Z. M., Yang, K.: *Adv. Mater. Res.*, 32, 2008, p. 207. [doi:10.4028/www.scientific.net/AMR.32.207](https://doi.org/10.4028/www.scientific.net/AMR.32.207)
- [21] Talbot, D. E. J., Talbot, J. D. R.: *Corrosion Science and Technology*. London, CRC Press 2007.
- [22] Atrens, A., Liu, M., Abidin, N. I. Z.: *Mater. Sci. Eng. B*, 2011. [doi: 10.1016/j.mseb.2010.12.017](https://doi.org/10.1016/j.mseb.2010.12.017).